

Generation and diagnostics of atmospheric pressure CO₂ plasma by laser driven plasma wind tunnel

メタデータ	言語: eng 出版者: 公開日: 2012-10-26 キーワード (Ja): キーワード (En): 作成者: Matsui, Makoto, Tanaka, Kensaku, Nomura, Satoshi, Komurasaki, Kimiya, Yamagiwa, Yoshiki, Arakawa, Yoshihiro メールアドレス: 所属:
URL	http://hdl.handle.net/10297/6839

Generation and diagnostics of atmospheric pressure CO₂ plasma by laser driven plasma wind tunnel

Makoto Matsui, Kensaku Tanaka, Satoshi Nomura, Kimiya Komurasaki, Yoshiki Yamagiwa et al.

Citation: *J. Appl. Phys.* **112**, 033301 (2012); doi: 10.1063/1.4739259

View online: <http://dx.doi.org/10.1063/1.4739259>

View Table of Contents: <http://jap.aip.org/resource/1/JAPIAU/v112/i3>

Published by the [American Institute of Physics](#).

Related Articles

Laser schlieren deflectometry for temperature analysis of filamentary non-thermal atmospheric pressure plasma
Rev. Sci. Instrum. **83**, 103506 (2012)

Reconstruction of polar magnetic field from single axis tomography of Faraday rotation in plasmas
Phys. Plasmas **19**, 103107 (2012)

Study of the plasma wave excited by intense femtosecond laser pulses in a dielectric capillary
Phys. Plasmas **19**, 093121 (2012)

Note: Statistical errors estimation for Thomson scattering diagnostics
Rev. Sci. Instrum. **83**, 096106 (2012)

Imaging spectroscopy diagnosis of internal electron temperature and density distributions of plasma cloud surrounding hydrogen pellet in the Large Helical Device
Rev. Sci. Instrum. **83**, 093506 (2012)

Additional information on J. Appl. Phys.

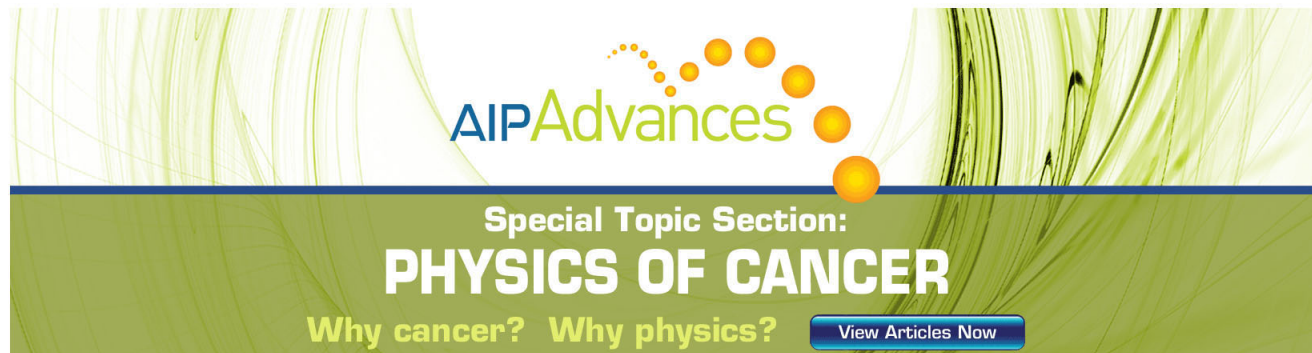
Journal Homepage: <http://jap.aip.org/>

Journal Information: http://jap.aip.org/about/about_the_journal

Top downloads: http://jap.aip.org/features/most_downloaded

Information for Authors: <http://jap.aip.org/authors>

ADVERTISEMENT



The advertisement banner features a green background with abstract, flowing lines. At the top, the text "AIPAdvances" is displayed in a stylized font, with "AIP" in blue and "Advances" in green. Below this, the text "Special Topic Section:" is written in white, followed by "PHYSICS OF CANCER" in large, bold, white capital letters. At the bottom, the text "Why cancer? Why physics?" is written in yellow, and a blue button with the text "View Articles Now" is located on the right side.

Generation and diagnostics of atmospheric pressure CO₂ plasma by laser driven plasma wind tunnel

Makoto Matsui,^{1,a)} Kensaku Tanaka,² Satoshi Nomura,³ Kimiya Komurasaki,³ Yoshiaki Yamagiwa,¹ and Yoshihiro Arakawa²

¹*Department of Mechanical Engineering, Shizuoka University, 3-5-4 Johoku, Naka, Hamamatsu, 432-8561 Shizuoka, Japan*

²*Department of Aeronautics and Astronautics, The University of Tokyo, 7-3-1 Hongo, Bunkyo, 113-0033 Tokyo, Japan*

³*Department of Advanced Energy, The University of Tokyo, 5-1-5 Kashiwanoha, Kashiwa, 277-8583 Chiba, Japan*

(Received 15 May 2012; accepted 14 June 2012; published online 1 August 2012)

Atmospheric pressure CO₂ plasma was generated by a laser driven plasma wind tunnel. At an ambient pressure of 0.38 MPa, a stable plasma was maintained by a laser power of 1000 W for more than 20 min. The translational temperature was measured using laser absorption spectroscopy with the atomic oxygen line at 777.19 nm. The measured absorption profiles were analyzed by a Voigt function considering Doppler, Stark, and pressure-broadening effects. Under the assumption of thermochemical equilibrium, all broadening effects were consistent with each other. The measured temperature ranged from 8500 K to 8900 K. © 2012 American Institute of Physics. [<http://dx.doi.org/10.1063/1.4739259>]

I. INTRODUCTION

Atmospheric pressure plasma has a wide variety of applications such as wear-resistance coating, cutting and fabrication of high melting point alloys, extreme ultraviolet (EUV) light sources, metal recovery, disposal of industrial waste, and simulation of atmospheric entry. The most frequently used plasma generation method is arc discharge. This is because, in addition to high-pressure operation up to 10 MPa, it has the advantages of a simple structure, long operational time, and ease of maintenance.¹ However, erosion of the electrodes causes flow contamination with an increase in pressure and also leads to unstable operation and eventually shutdown when active gases are used.²

To avoid this, generators that have no electrode such as inductively coupled plasma (ICP) and microwave generators have garnered much attention.^{3,4} They can produce very low contamination flows because their flows have no undesirable chemical reactions resulting from electrode erosion. Another advantage of such generators is that they can use even reactive gases such as carbon dioxide and oxygen because of their electrodeless heating. However, plasma instability limits the operation pressure of these generators to less than atmospheric. As a result, a stationary plasma at a pressure higher than atmospheric is difficult to produce.⁵ This is partly because of the cut-off phenomenon. The electron density corresponding to the cutoff frequency is less than 10^{17} m^{-3} even at a microwave frequency of 2.45 GHz. This problem also causes an extremely low degree of ionization and an upper temperature limit around 6000 K under atmospheric conditions.⁶

Laser sustained plasma (LSP) is one of the most promising methods for overcoming the above problems using

high-pressure plasma generation. In LSP, the plasma is sustained by absorbing focused laser beam power through an inverse bremsstrahlung radiation process between electrons and ions.⁷ Therefore, it has the advantages of electrodeless heating such as clean flows and availability of active gases. Additionally, it has two more advantages: One is the operation pressure. In our previous research, argon LSP was successfully generated at pressures of up to 1 MPa.⁸ The other is the plasma position. In the case of ICP or microwave plasma, the plasma core is generated in an induction coil or a cavity, which means that the high-temperature core region is not convenient for applications. On the other hand, the core region of the LSP can easily be moved by changing a focal lens position through the window because it is generated around the focal position.⁹ Then, the core region is available for any purpose.

Our ultimate goal is simulations of Mars and Venus entry conditions to investigate thermo-physical and radiative properties around entry vehicles. A main constituent in these atmospheres is carbon dioxide (CO₂). In addition, during Venus entry by the Pioneer Venus probe in 1978, the impact pressure was up to 0.7 MPa at maximum heat flux altitude.¹⁰ Such conditions cannot be simulated by conventional ICP or microwave generators. In this study, the conditions necessary to generate atmospheric pressure CO₂ plasma in a laser driven plasma wind tunnel were investigated. In addition, the translational temperature of the LSP was measured by laser absorption spectroscopy (LAS).

II. EXPERIMENTAL THEORY

A. Absorption coefficient and number density

LAS is applicable to optically thick plasma and does not require absolute calibration using a calibrated light source or a density reference cell such as in emission spectroscopy and

^{a)}Author to whom correspondence should be addressed. Electronic mail: tmmatui@ipc.shizuoka.ac.jp.

laser induced fluorescence.¹¹ In addition, measurement systems using a diode laser can be portable.¹² In this study, absorption profiles are measured for the transition of 3s5S to 3p5P, which is a metastable state of atomic oxygen (OI) at 777.19 nm.

The relationship between probe laser intensity $I(\nu)$ and absorption coefficient $k(\nu)$ is expressed by the Beer-Lambert law as

$$\frac{I(\nu)}{I_0(\nu)} = \exp\left(-\int k(\nu)dx\right). \quad (1)$$

Here, ν is the laser frequency, I_0 is the incident laser intensity, and x is the coordinate in the laser pass direction.

Assuming the Boltzmann relation between absorbing and excited states, the integrated absorption coefficient K is expressed as a function of the number density at the absorbing state n_i as

$$K = \int_{-\infty}^{\infty} k(\nu)d\nu = \frac{\lambda^2}{8\pi} \frac{g_j}{g_i} A_{ij} n_i \left[1 - \exp\left(\frac{\Delta E_{ij}}{kT_{\text{ex}}}\right)\right]. \quad (2)$$

Here, subscripts i and j denote the absorbing and excited states, respectively. In addition, λ , g , A , ΔE , k , and T_{ex} are the absorption wavelength, statistical weight, Einstein coefficient, energy gap between the states, Boltzmann constant, and electronic excitation temperature, respectively. Transition data for the target absorption line are listed in Table I.¹³

B. Line broadening

The absorption profile is broadened by various physical mechanisms and is expressed by a convolution of the Gauss and the Lorentz distributions. Brief derivations and results are presented here.^{14–16}

1. Doppler broadening

The Doppler effect is observed to shift the proper frequency of a moving atom, resulting in a broadening of the profile. This is called Doppler broadening. This broadening is a Gaussian distribution, and its width $\Delta\nu_D$ is related to the translational temperature T_{tr} as

$$\Delta\nu_D = \frac{2\nu_0\sqrt{\ln 2}}{c} \sqrt{\frac{2k_B T_{\text{tr}}}{M_A}}. \quad (3)$$

Here, ν_0 , k_B , M_A , and c are the center absorption frequency, Boltzmann constant, atomic weight, and velocity of light, respectively.

2. Pressure broadening

Pressure broadening originates from the fact that atoms are perturbed by collisions with other atoms or molecules.

TABLE I. Transition data for the target absorption line.

i	j	λ , nm	E_i , eV	E_j , eV	g_i	g_j	A_{ji} , 10^8 s^{-1}
3s ⁵ S	3p ⁵ P	777.19	9.14	10.7	5	7	0.369

This broadening is a Lorentz distribution and its width $\Delta\nu_p$ is expressed as

$$\Delta\nu_p = n \left(\frac{9\pi\hbar^5 \nu_0 \overline{R_\alpha^2}}{16m_e^3 E_p^2} \right) v^{-\frac{3}{5}} \times 10^{-9}. \quad (4)$$

Here, \hbar , $\overline{R_\alpha^2}$, m_e , E_p , and v are the reduced Planck constant, square of the coordinate vector of the radiating electron, electron mass, perturbed resonance-level excitation energy, and thermal velocity, respectively.

3. Stark broadening

Stark broadening originates from the fact that the degeneracy is solved by the electric field made by a surrounding electron. This broadening is a Lorentz distribution also, and its width w_{th} is expressed as

$$w_{\text{th}} \approx 2 \left(1 + 1.75 \times 10^{-4} n_e^{1/4} \alpha (1 - 0.068 n_e^{1/6} T_e^{1/2}) \right) n_e w \times 10^{-18}. \quad (5)$$

Here, n_e , α , and w are the electron number density, ion broadening parameter, and electron impact parameter, respectively.

4. Other types of broadening

Natural, saturation, and transit time broadening are more than two orders of magnitude smaller than the above three types of broadening. Therefore, they are not considered here.

C. Line shape function and analytical method

The actual absorption profile is the convolution of the Gauss and the Lorentz function. This profile is called the Voigt profile and is expressed as

$$k(\nu) = \frac{k(\nu_0)}{\pi\Delta\nu_L} \int_{-\infty}^{\infty} \frac{\exp\left\{-\left(\frac{2\delta}{\Delta\nu_D} \sqrt{\ln 2}\right)^2\right\}}{1 + \left\{\frac{2(\nu-\nu_0-\delta)}{\Delta\nu_L}\right\}^2} d\delta. \quad (6)$$

Here, $\Delta\nu_L$ is the sum of the Lorentz widths shown in Eqs. (4) and (5) and δ is the integration variable.

In this study, the ambient pressure is more than that of the atmosphere, and the flow is subsonic; therefore, the plasma is assumed to be in thermochemical equilibrium. Then, using an equation of state and the Saha equation, the pressure and the Stark broadenings become functions of the temperature. However in practice, a curve fitting of Eq. (6) to the measured profiles after substituting by Eqs. (3)–(5) is too difficult because of the complexity of the function.

Therefore, in this study, the absorption profiles were analyzed by the following process. First, the Lorentz width, which is the sum of the pressure and Stark widths, is calculated by a given Lorentz temperature T_L . Next, the Voigt function is fitted to the profiles with the calculated Lorentz width and variable Doppler width. Then, the temperature

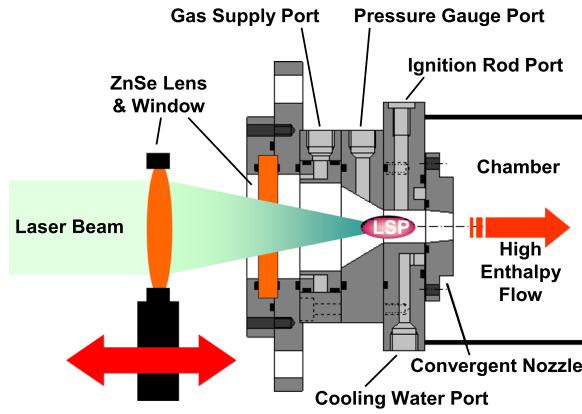


FIG. 1. Cross-sectional diagram of the laser driven plasma wind tunnel.

from the obtained Doppler width T_D is compared with the Lorentz temperature by the performance function S

$$S = \left(\frac{T_L - T_D}{T_L} \right)^2. \quad (7)$$

When the performance function is at a minimum, the Lorentz temperature will be the true temperature.

III. EXPERIMENTAL APPARATUS

A. Laser driven plasma wind tunnel

A cross-sectional diagram and a photo of the LSP wind tunnel are presented in Figs. 1 and 2, respectively. The LSP generator is composed of a laser induction window, a plasma-sustaining channel, and a convergent nozzle. The throat diameter is 12 mm and the nozzle diameter is 10 mm. With this slightly convergent configuration, the LSP can be sustained at the nozzle exit. As a beam source, a continuous wave CO₂ laser (YB-L200B7T4, Matsushita Electric Industrial Co., Ltd.) with a wavelength of 10.6 μm is used. The maximum output power is 2 kW and the transverse mode of the laser beam is TEM₁₀. The beam divergence is less than 2 mrad at the laser exit. The beam diameter of 20 mm is magnified by a factor of 2.2 using a ZnSe beam expander, and the expanded beam is condensed into the generator by a ZnSe meniscus lens (P/N 61853, Ophir Optronics Ltd.) through a ZnSe window. The focal length of the lens is 95 mm, corresponding to an F-number of 1.9, which is defined as the focal length normalized by the beam diameter.

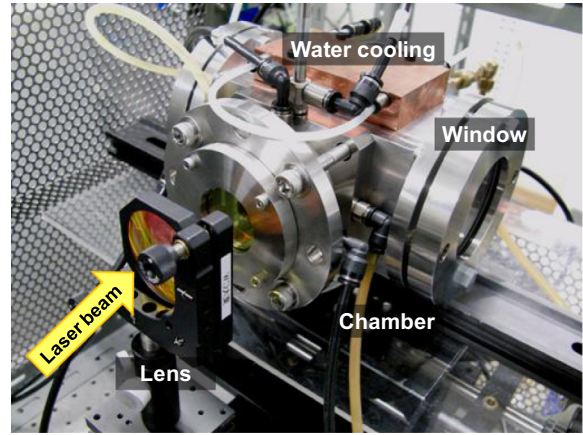


FIG. 2. Photo of the laser driven plasma wind tunnel.

This lens can move back and forth in the laser beam direction using a traverse stage. A rod made of stainless steel (SUS304) is used as the source of the initial electron emission. After the ignition, the LSP is moved toward the nozzle exit by moving the focal lens position. The generator is connected to a water-cooled high-pressure chamber with two quartz windows for optical diagnostics. The chamber is evacuated through the 1 mm throat by a rotary vacuum pump (VD401, ULVAC Technologies, Inc.).

B. Measurement system

Figure 3 shows a schematic of the LAS measurement system. A tunable diode laser with an external cavity (Velocity Model 6300, New Focus, Inc.) is used as the laser oscillator. Its line width is less than 500 kHz and the laser frequency is scanned over the absorption line shape. The modulation frequency and width were 0.5 Hz and 30 GHz, respectively. An optical isolator is used to prevent the reflected laser beam from returning into the external cavity. An etalon with a free spectral range of 0.75 GHz is used to calibrate relative frequency. Microwave discharge plasma is used as a reference cell to adjust the laser frequency to the absorption peak.

The probe beam diameter is 1 mm, and the beam is guided to the chamber window through a single mode optical fiber. The fiber output is mounted on a two-dimensional traverse stage to scan the flow in the radial and axial directions. To reduce plasma emission, the transmitted laser intensity is measured by a photo detector (DET110/M, Thorlabs, Inc.)

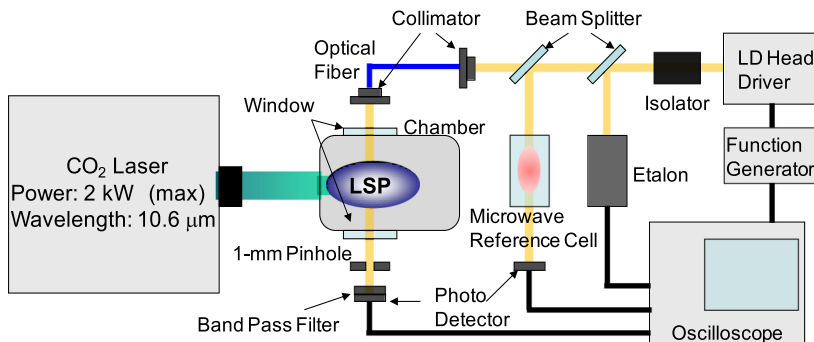
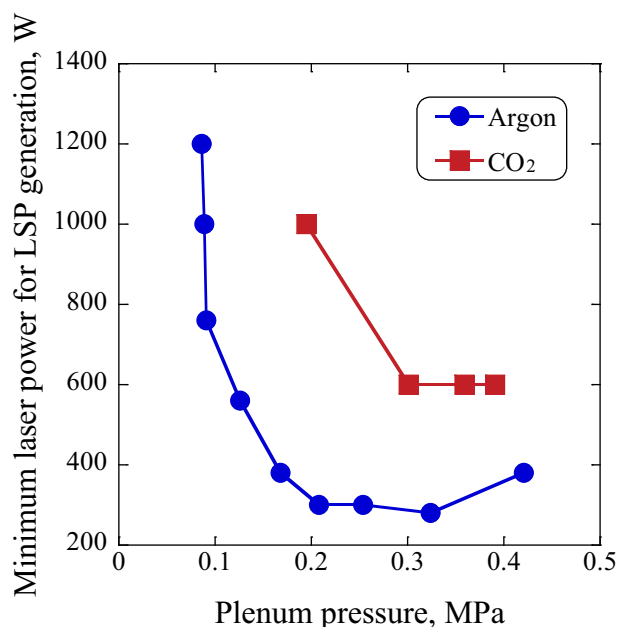


FIG. 3. Schematic of LAS measurement system.

FIG. 4. Generating conditions for CO₂ and argon LSP.

with a 2-mm pinhole and a band-pass filter whose full width at half maximum is 10 nm (FB770-10, Thorlabs, Inc.). The signals are recorded using a digital oscilloscope with 16-bit resolution at a sampling rate of 10 kHz (Yokogawa DL1540; Yokogawa Electric Corp.).

IV. RESULTS AND DISCUSSION

A. Generating conditions

Figure 4 shows the minimum laser power for LSP generation as a function of plenum pressure. For comparison, the minimum laser power of argon is also plotted. Here, the pressure represents cold gas values. As seen in this figure, the LSP can be generated with less laser power at higher pressure. The minimum laser power for the CO₂ LSP generation is around 600 W, which is much higher than that needed for argon. This is because the dissociation energy is necessary for the molecular flow to generate enough electron density to maintain the LSP. In this study, the upper limit of the pressure is determined by the gas regulator system because the heating system is necessary only for CO₂ operation. Therefore, with the higher power heater, the CO₂ LSP would be generated at a higher pressure by comparable laser power. Figure 5 shows a typical photo of the CO₂ plasma flow. By moving the focal lens downstream, the LSP flow can be stably produced at the nozzle exit.

B. Temperature measurements

The operating conditions are tabulated in Table II. Under these conditions, the plasma was maintained for more than 20 min. Figure 6 shows a typical distribution of OI 777 nm line emission intensity. An extremely strong peak was observed. This peak is thought to be the LSP core position, where most of the laser beam is absorbed.¹⁷ The LSP position is not the same as the focal point but depends on

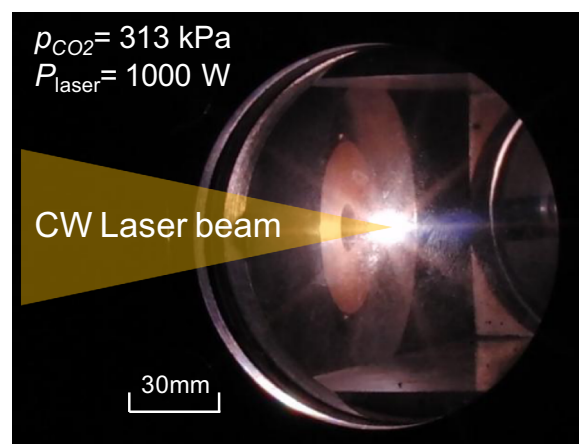
FIG. 5. Photo of CO₂ plasma flow.

TABLE II. Operating conditions.

No.	1	2	3
Laser power, W	1000	1000	1400
Mass flow rate, g/s	0.39	0.46	0.39
Pressure, MPa	0.313	0.383	0.323

operating conditions such as ambient pressure, flow velocity, and laser power.¹⁸ We therefore set the coordinate origin not to the focal point, but to the peak point of the OI 777 nm line intensity.

Figure 7 shows typical absorption signals. The absorption signal could be detected at the front of the LSP, where the temperature was highest. At 0.5 mm away from the position in the radial and axial direction, no absorption signal was observed. This result is consistent with the emission distribution shown in Fig. 6. Then, the obtained absorption signal is assumed to give the local absorption coefficient on the origin for an absorption length of 0.5 mm. However, note that the measured transmitted laser intensity generally gives only the

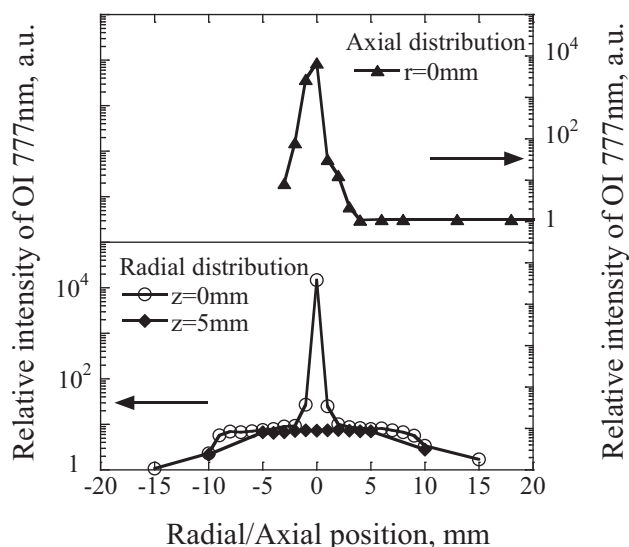


FIG. 6. Emission intensity distribution of OI 777-nm line.

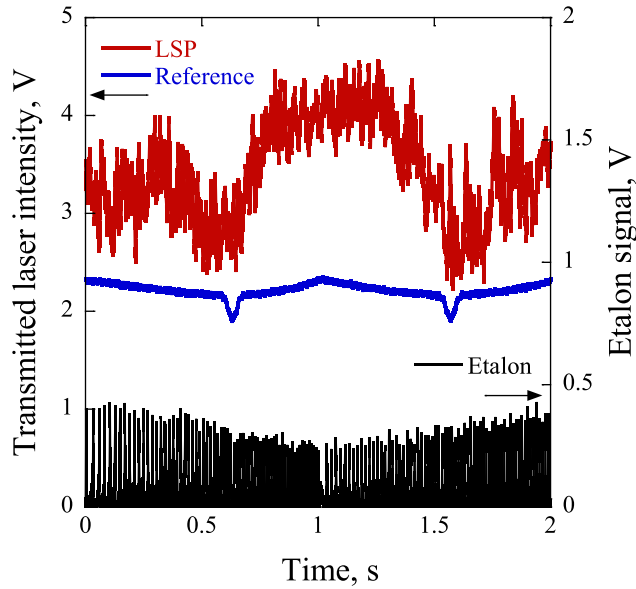


FIG. 7. Typical transmitted laser intensity in the LSP and microwave plasma and etalon signal.

path-integrated absorption coefficient; Abel inversion is necessary to determine the local absorption coefficient.

For the normalized absorption signals, the Voigt function was fitted as described in Sec. II. Figures 8 and 9 show how a typical performance function varies with the Lorentz temperature and the absorbance with a fitted curve. As shown in these figures, the performance function has a minimum, and the Voigt function is well fitted to the measured profile. In all conditions, the performance functions have a minimum, and their values are less than 0.03.

Figure 10 shows the measured temperature, which ranged from 8500 K to 8900 K. The temperature decreased with the increase in pressure. This might be because that the radiation loss increases with an increase in pressure.¹⁸ Increasing laser power from 1000 to 1400 W increased the

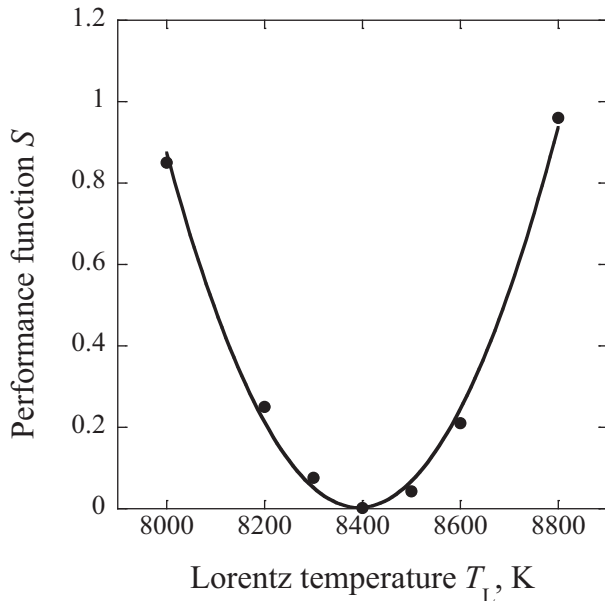


FIG. 8. Variation in performance function with Lorentz temperature.

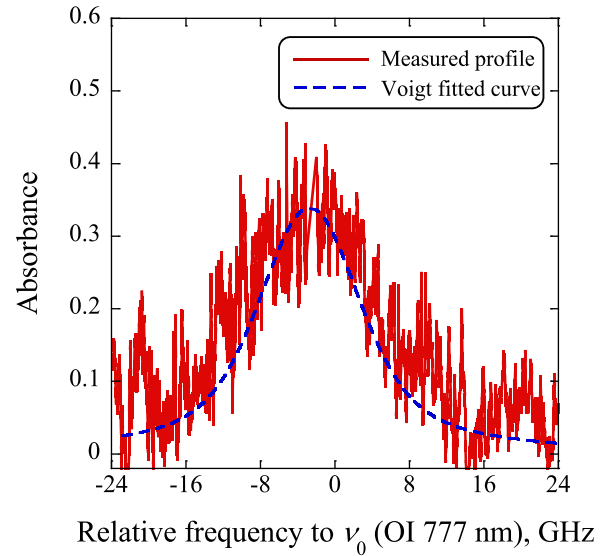


FIG. 9. Typical absorbance and Voigt fitted curve.

temperature only slightly. In our previous research,¹⁹ the LSP position was found to move upstream from the focal point with an increase in laser power. Thus, the laser intensity at the front of the LSP does not increase even if the laser power is increased. As a result, with the increase in laser power, the temperature increases are slight even though the front area of the LSP increases in the radial direction.

C. Validation of thermochemical equilibrium

Assuming that the LSP is in local thermal equilibrium, the number density of the absorbing state is related to the number density of atomic oxygen n_O by the Boltzmann distribution law, expressed as

$$n_i = \frac{n_O g_i \exp(-E_i/k_B T_{ex})}{\sum_k g_k \exp(-E_k/k_B T_{ex})}. \quad (8)$$

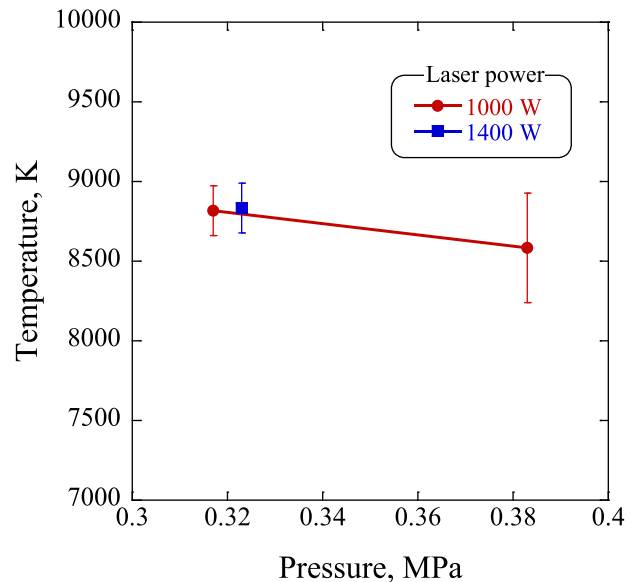


FIG. 10. Measured temperature as a function of pressure.

Here, the summation is conducted for the ground and all excited states of atomic oxygen. Around the measured temperature, the CO₂ gas is completely dissociated into carbon and atomic oxygen under the thermochemical equilibrium. The number density of atomic oxygen can then be obtained by the equation of state. In the case of the no.1 condition, the number density of the absorbing state based on these equations is estimated as $1.1 \times 10^{19} \text{ m}^{-3}$. On the other hand, the number density measured by LAS is $1.3 \times 10^{19} \text{ m}^{-3}$. These values show good agreement. Hence, it is reasonable to assume the LSP is in thermochemical equilibrium.

V. CONCLUSION

Atmospheric CO₂ plasma flows were generated by the laser driven plasma wind tunnel. The plasma was maintained stably for more than 20 min at a pressure of up to 0.4 MPa. As a result of the flow diagnostics measured by laser absorption spectroscopy, the temperature at the front of the LSP was found to range from 8500 K to 8900 K, where the plasma was in thermochemical equilibrium.

ACKNOWLEDGMENTS

This research was partially supported by the Ministry of Education, Science, Sports and Culture, Grant-in-Aid for Young Scientists (A), Grant No. 22686079, 2010.

- ¹M. A. Birkan, *J. Propul. Power* **12**, 1011 (1996).
- ²M. Matsui, T. Ikemoto, H. Takayanagi, K. Komurasaki, and Y. Arakawa, *J. Thermophys. Heat Transfer* **21**, 247 (2007).
- ³M. Matsui, K. Komurasaki, Y. Arakawa, A. Knapp, G. Herdrich, and M. Auweter-Kurtz, *J. Spacecr. Rockets* **45**, 155 (2005).
- ⁴P. P. Woskov, D. Y. Rhee, P. Thomas, D. R. Cohn, and J. E. Surma, *Rev. Sci. Instrum.* **67**, 3700 (1996).
- ⁵T. Yamada, K. Fujita, S. Nonaka, and N. Ishii, in *Proceedings of ISTS* (2006), p. e-19.
- ⁶Y. Babou, P. Riviere, M. Y. Perrin, and A. Soufiani, *Plasma Sources Sci. Technol.* **17**, 045010 (2008).
- ⁷R. Conrad, Y. P. Raizer, and S. T. Sarzhikov, *AIAA J.* **34**, 1584 (1996).
- ⁸M. Matsui, K. Shinmi, T. Ueno, K. Komurasaki, and Y. Arakawa, *Trans. JSASS, Aerospace Technol. Jpn.* **7**, 31 (2009).
- ⁹M. Matsui, S. Yamagishi, K. Komurasaki, Y. Yamagiwa, and Y. Arakawa, *Trans. JSASS, Aerospace Technol. Jpn.* **8**, 31 (2010).
- ¹⁰C. Park and H. K. Ahn, *J. Thermophys. Heat Transfer* **13**, 33 (1999).
- ¹¹W. Demtroder, *Laser Spectroscopy*, 2nd ed. (Springer Verlag, Berlin, 1996).
- ¹²M. Matsui, K. Komurasaki, G. Herdrich, and M. Auweter-Kurtz, *AIAA J.* **43–49**, 2060 (2005).
- ¹³NIST Atomic Spectra Database, Available at <http://www.nist.gov/pml/data/asd.cfm>.
- ¹⁴R. H. Huddleston and S. L. Leonard, *Plasma Diagnostic Techniques* (Academic, New York, 1965).
- ¹⁵M. Mitchner and C. H. Kruger, *Partially Ionized Gases* (Wiley-Interscience, New York, 1973).
- ¹⁶H. Griem, *Plasma Spectroscopy* (McGraw-Hill, New York, 1964).
- ¹⁷K. Komurasaki, P. M. Morales, K. Toyoda, and Y. Arakawa, *Trans. Jpn. Soc. Aeronaut. Space Sci.* **44**, 65 (2001).
- ¹⁸J. P. Jackson and P. E. Nielsen, *AIAA J.* **12**, 1498 (1974).
- ¹⁹T. Inoue, T. Ijiri, S. Hosoda, K. Kojima, S. Uehara, K. Komurasaki, and Y. Arakawa, *Vacuum* **73**, 433 (2004).